

INVITED DISCOURSES

THE HUBBLE DEEP FIELD

ROBERT WILLIAMS
Space Telescope Science Institute
Baltimore, MD, USA

1. Introduction

Great progress has been made in recent years in understanding the large-scale structure of the universe. Recall that it is only within this century that we have even come to realize the existence of other galaxies as separate entities. Until the 1920's the universe did not extend beyond the Milky Way. Novae and Cepheid variables changed that picture, and for the past 75 years extragalactic astronomy has been one of the most active and fertile areas of science. The concept of an expanding universe and its beginning in a Big Bang all derive from the discovery of external galaxies.

Distant galaxies are faint and have small angular sizes, therefore their study has remained the province of the largest telescopes. Before the launch of Hubble Space Telescope, ground-based telescopes had succeeded in detecting distant galaxies out to redshifts of $z \sim 1$, and in establishing certain of their characteristics. But, there was uncertainty as to how much further HST could push the study of distant galaxies given its modest 2.4m diameter mirror and the fact that the surface brightnesses of cosmologically distant objects decrease as $(1+z)^4$.

For this reason, one of the early observations that was scheduled immediately after the first servicing mission of HST in December 1993 to repair spherical aberration was the re-imaging of the cluster of galaxies 0939+4713 at $z = 0.4$ that had been observed previously by Dressler et al. (1994) from both the ground and with the aberrated HST. The ten-orbit WFPC2 image demonstrated HST's ability to resolve structure in distant galaxies, showing spiral and elliptical galaxies with a clarity approaching that achieved for the Coma cluster from the ground. Spirals are seen to be relatively abundant in 0939+4713, although they generally show an anomalous morphology.

The 0939+4713 observation was followed some months later by a GO program of Dickinson (1995) to image for 32 orbits the strong radio galaxy 3C 324 at redshift $z = 1.2$. The final combined image of 3C 324 and associated galaxies was very interesting in that it revealed numerous ellipticals, but unlike 0939+4713, no spiral galaxies. Furthermore, the E's were measured to have a $r^{1/4}$ radial light distribution characteristic of dynamically relaxed stellar systems. The ellipticals thus showed evidence of already being old at this higher redshift, whereas spiral galaxies were not yet present. The extent to which this difference in the two clusters indicated basic evolutionary properties of E's and S's was difficult to ascertain because of the small sample involved of only two clusters. However, it did demonstrate the power of HST to discern galaxy structure at high redshift.

2. The HDF Campaign

Following informal discussions among the Institute scientific staff on what additional observations HST might undertake that would make an important contribution to our understanding of galaxy evolution, the decision was taken to devote a substantial fraction of Director's Discretionary time in Cycle 4 to this topic. Certain desired characteristics of any deep image were agreed upon by us, and these included (1) selecting fields with low extinction, known to include distant galaxies, (2) observing in the HST Continuous Viewing Zone to maximize observing time, (3) obtaining color information by imaging in at least 2 wavelength bands, (4) setting the total exposure time so the background noise would be reduced below CCD systematic noise levels, (5) dithering the exposures to recover sub-pixel spatial resolution, (6) imaging the flanking fields around any primary field to provide an HST image that matched the field size of ground-based telescopes, and (7) making the

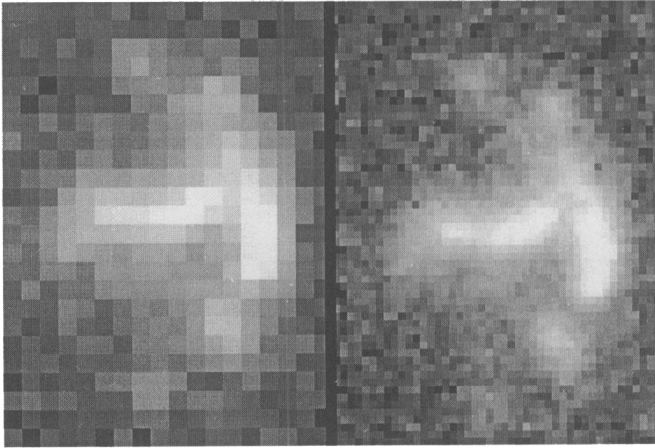


Figure 1. Comparison of two combined images of an object in the HDF, produced from the same dataset using different procedures. The left image is the result of the shift-and-add technique, and the right image is the result of 'drizzling' (from Fruchter & Hook 1997).

data non-proprietary as soon as it could be properly reduced so it would be available immediately for broad community study and follow-up.

What our discussions did not satisfactorily resolve was which fields should be imaged. An external advisory committee was therefore convened to define appropriate programs that could be executed. They agreed with most of the desirable characteristics that had been set forth, but strong discussion focused on what field(s) should be studied. The majority favored selection of a few targeted fields with known high-redshift galaxies, as opposed to several committee members who insisted that a deep study of one or two random, representative fields would yield the most significant results. Arguments pro and con were intensively debated throughout the day until the inability of the majority to agree upon which fields to target took its toll! At this point, the minority argument of simply selecting a random field took on greater credibility, and eventually was what was decided upon.

A group of scientists at ST ScI formed a team to identify a field and execute a deep image, which we called the Hubble Deep Field (HDF). The field eventually selected was a random one that was chosen in the northern CVZ that fit all the above criteria, and whose specific coordinates were dictated by the presence of independent pairs of HST guide stars. The observations were carried out over a two week period in December 1995, with 342 dithered exposures obtained over 150 consecutive orbits in the four WFPC2 broad-band filters F300W, F450W, F606W, and F814W (Williams et al. 1996). The flanking fields were also imaged in the I band for 1–2 orbits each.

The individual exposures in each passband were cleaned and combined by a process that was developed for this observing procedure by Fruchter & Hook (1997) called Variable Pixel Linear Reconstruction (VPLR), or 'drizzling'. VPLR maps the detector input pixels, whose sizes are arbitrarily shrunken to a smaller size commensurate with the dither pattern, onto an output grid whose pixel size is chosen to match that of the telescope resolution and the dither scheme. The flux assigned to each output pixel is the sum of the fluxes of the various input pixels that are mapped onto that output pixel, weighted by the fractions of the area of each input pixel that overlap that output pixel. It is as if the input flux drizzled down onto the output grid, hence the name 'drizzling' given to this technique. It is an excellent procedure for registering dithered data in the presence of geometrical distortion of the detector, and it conserves both flux and surface brightness. Drizzling does not treat background noise optimally, but it is an excellent method to recover spatial resolution lost by detector undersampling. Fig. 1 shows a comparison of a feature from the HDF dataset that has been combined by two techniques, shift-and-add vs. drizzling, and the improved resolution yielded by drizzling is apparent.

A gray-scale image of the final HDF produced by combining the exposures from the B, V,

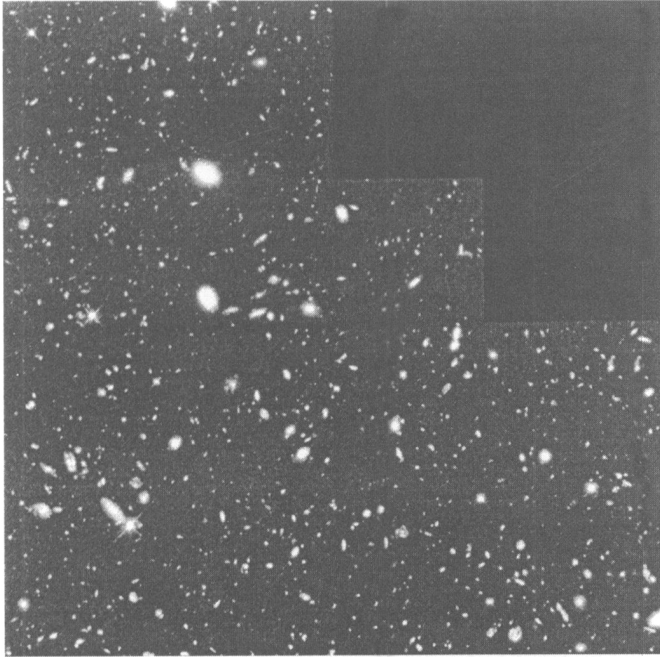


Figure 2. Gray-scale composite drizzled image of the HDF, obtained from combining the majority of individual dithered exposures in B, V, and I bands

and I bands is shown in Fig. 2 on a logarithmic intensity scale to enhance the detail visible at all brightness levels. The faintest sources have brightnesses of about $V = 29^m$, and there are more than 2,000 identifiable objects in the image, most of which are extragalactic. No solar system objects appear in the combined HDF image since any such object would display motion during the observing sequence, and the cosmic ray cleaning algorithm therefore treats them as artifacts and rejects them. The objects in the HDF thus consist of galactic stars and galaxies, and the distinction between these two classes can generally be made from their image sizes, compared with the point spread function (PSF). Distance determinations for the sources are the most important information necessary for interpretation of the data, and these require follow-up spectroscopy, but some conclusions can be drawn without knowledge of the specific object distances.

3. The Stellar Component

Study of the stars in the HDF provides constraints on the stellar luminosity function at faint magnitudes, and several groups have worked on this problem beginning with the identification of the galactic stars. Elson, Santiago, & Gilmore (1996=ESG) and Gould, Bahcall, & Flynn (1997=GBF) each determine the image size for all objects in the HDF down to $V = 28^m$, the limit at which noise makes discrimination of a stellar from a non-stellar object problematical. A color-magnitude diagram of all stellar-like objects in the HDF is shown in Fig. 3, taken from ESG. There are two grouping of objects: one of which is blue and consists of 50 sources, and another which is red, consisting of about 10 objects. The blue group is too blue to be anything but white dwarfs if they are indeed stars, and their brightnesses then require them to all have distances of about 10 kpc. Any realistic model of the Galaxy leads one to expect even more WD's at closer distances, but such objects do not appear in the CM diagram. The hypothesis that these objects are WD's must therefore be rejected, and the blue objects, which are all fainter than 26th magnitude, must reasonably be considered to be point-like extragalactic objects. This leaves the 9 reddish objects as the only likely stars in the HDF down to $V = 28^m$.

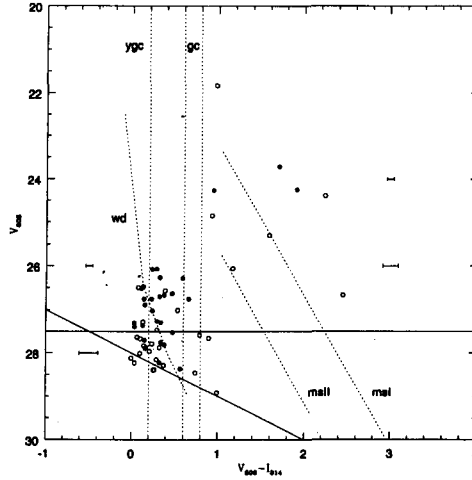


Figure 3. Color-magnitude diagram of all stellar-like objects in the HDF brighter than $V = 28^m$ (from ESG 1996).

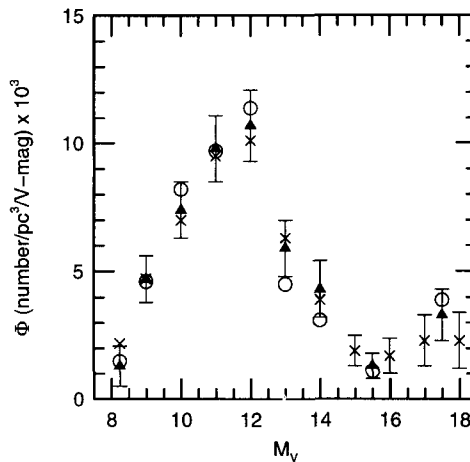


Figure 4. Stellar luminosity function derived from HST data including the Groth Strip. Note the pronounced turn down for luminosities fainter than $M_v = 12$ (from GBF 1997).

Three different groups (ESG; GBF; Mendez et al. 1996) have taken the HDF stellar data and fitted them to models of the Galaxy in order to determine properties of the disk and halo. The specifics of their procedures and conclusions differ, but they agree on the basic finding concerning the stellar luminosity function: it must turn down for magnitudes fainter than $M_v = 12$, as can be seen in Fig. 4, from GBF—a result of some significance.

4. Galaxy Number Counts

Turning our attention to the galaxies in the HDF, one of the fundamental relations that can be determined is that of galaxy numbers per unit magnitude interval. Number counts have been obtained straightforwardly for the HDF from photometry of the sources in the different passbands, and the results for the B and I bands are shown in Fig. 5. The HDF results are seen to agree

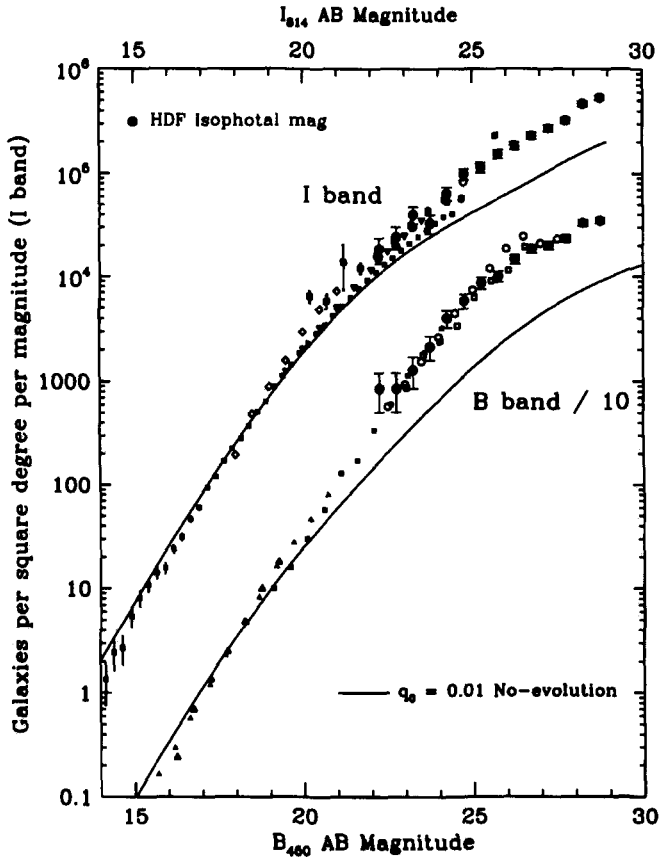


Figure 5. Galaxy number counts in the HDF from the B and I bands, compared with ground-based results and non-evolving model predictions (from Ferguson & Babul 1997).

with previous ground-based results at brighter magnitudes where there is overlap, and to smoothly extend beyond them at fainter magnitudes. Of interest is the comparison of the data with the relationship predicted for a non-evolving galaxy luminosity function, shown by the solid line in Fig. 5. The actual data exceed the expected counts at fainter magnitudes in both B and I, with the discrepancy being greatest in the blue. This is the origin of the well known 'faint blue galaxy' excess that has prompted certain scenarios for the recent evolution of galaxies such as the existence of dwarf galaxy bursts at epochs $0.5 < z < 1$ (Ferguson & Babul 1997). Clearly, the data require either the numbers or the luminosities of galaxies to have changed in relatively recent times although the number counts alone do not dictate which alternative is correct.

5. HDF at other Wavelengths

The HDF has now been imaged in wavelength regions other than the optical, and sources have been identified with the optical galaxies. Roughly 100 hours of radio mapping of the HDF and flanking fields has been done at 8 GHz using the VLA by Kellermann, Fomalont, and colleagues, in which they achieved a detection threshold of $10 \mu Jy$ and a spatial resolution of 4 arcsec (Fomalont et al. 1997). They find seven sources, of which six can be identified with galaxies visible in the HDF image. Three of the radio sources are associated with red elliptical galaxies of redshift $z \sim 1$ and

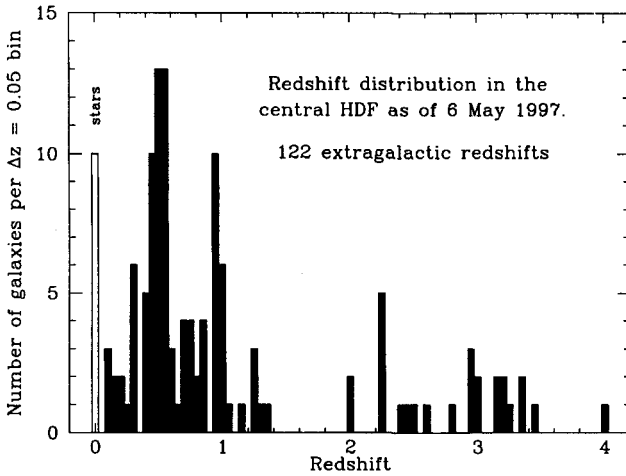


Figure 6. Histogram of spectroscopic redshifts for HDF objects measured by the various consortia with the Keck 10m + LRIS. Smaller redshifts are from the magnitude-limited samples, and larger redshifts are from the U- and B-band dropout samples. (Compiled from available data in the literature and websites by M. Dickinson).

having normal appearance. The other three sources are identified with disk galaxies of intermediate redshift, $z \sim 0.5$, and in each case there are indications of interactions with nearby galaxies, as if radio emission in disk systems is stimulated by interactions and mergers. One remaining weak radio source has no corresponding optical counterpart and may represent a galaxy enshrouded in dust or having such a high redshift ($z > 6$) that the Lyman limit is longward of the I band, i.e., an I-band dropout.

ESA's ISO observatory has also devoted 12.5 hours of time to image the HDF with its ISO-CAM at 6.7μ and 15μ . Two groups, from Imperial College London and Saclay, are analyzing the data (Serjeant et al. 1997; Cesarsky et al. 1997), and their studies have identified sources down to a $100\mu Jy$ detection threshold with a 6-12 arcsec resolution. They find a strong correlation between the sources at each of the IR wavelengths and also between the ISO and the VLA radio sources. They interpret the IR emission to be due to dust (primarily PAH's) and to stellar winds associated with an old stellar population.

6. Redshift Distribution

The excellent spatial resolution and depth of the HDF have caused this field to be chosen for intensive ground-based follow-up study. In particular, groups having access to the Keck 10m telescopes have committed considerable time and resources to obtaining redshifts for as many of the HDF sources as possible, to aid in the interpretation of the HST imaging. Furthermore, the different research groups have coordinated their spectroscopic programs in order to eliminate duplication and they have made most of the redshifts available to the community before publication. At the present time, after two observing seasons, 122 galaxy redshifts have been obtained within the HDF, and their distribution is shown in Fig. 6.

The histogram of redshifts consists basically of two distinct samples. The first is the approximate magnitude-limited sample of the Keck consortia, which have obtained spectra of HDF objects down to $R = 24^m$, and the second is the group of U-band dropouts that were selected on the basis of their likely having high redshift. Almost all of the objects with $z < 1.5$ belong to the magnitude-limited sample, and the $z > 1.5$ objects belong to the second, color-selected sample. The non-uniformities, or peaks, in the redshift distribution are statistically significant, and the median redshift of $\langle z \rangle \sim 0.5$ for the magnitude-limited sample is consistent with the findings of ground-based studies such as the CFRS (Lilly et al. 1996).

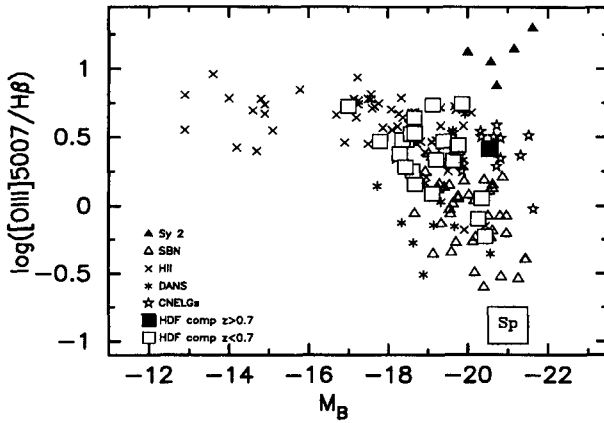


Figure 7. Relation between [O III]/ $H\beta$ flux vs. absolute blue magnitude for compact galaxies in the HDF. The galaxies have intermediate redshifts and moderately strong emission lines. They occupy the same region of the diagram as starburst galaxies, as opposed to other types of active galaxies (from Guzman et al. 1997).

The morphologies of the objects in the HDF are related to their redshifts. Normal Hubble sequence galaxies are seen primarily at low redshifts, whereas a very high fraction of objects with $z > 1$ have disturbed morphologies and evidence for interactions (Abraham et al. 1996). This is especially borne out by the appearances of the U-band dropout sample, which are all irregular and disturbed (Steidel et al. 1996). Colley et al. (1996) have determined the 2-point correlation function for HDF galaxies, and they find that the function increases for object separations of 2 arcsec or less, especially for the U-band dropout sample, which are primarily at high redshifts. This indicates either a high rate of interactions and mergers or the fact that closely separated HDF objects may in fact be simply the visible, higher surface brightness components of an underlying galaxy.

7. Spectroscopic Follow-Up Results

The 'DEEP' collaboration at Lick/UCSC has studied three separate samples of galaxies in the HDF and flanking fields, for which they have obtained Keck 10m LRIS spectroscopy. The first sample consists of the brighter ($I < 23.7^m$), higher surface brightness, compact (half-light radius < 0.5 arcsec) objects in the flanking fields. They identify 61 such galaxies, having a range in redshifts of roughly $0.4 < z < 1$ (Guzman et al. 1997). For these objects they find that the spectra consistently show strong emission lines, particularly [O II] 3727, with an H&K break and a blue continuum. The [O II] strengths point to star formation rates of $0.1\text{--}10 M_{\odot}/\text{yr}$, and the line widths indicate that these compact systems are more massive than present day dwarf galaxies. The relationship between [O III] 5007/ $H\beta$ vs. absolute blue magnitude for these compact galaxies, shown in Fig. 7, is identical to that of present day starburst galaxies, as opposed to Liners, Seyferts, or other types of active galaxies.

The second sample consists of isolated disk galaxies brighter than $I = 22.5^m$ and with inclinations $i > 30^{\circ}$. There are 8 such systems which have redshifts in the range $0.15 < z < 0.75$, and Keck spectra of them were taken with the slit oriented along the major axes so that rotation curves were obtained for the galaxies (Vogt et al. 1997). The velocity turnovers were observed for most of the galaxies, and the results modeled in order to determine the mass distributions and M/L ratios. The corresponding Tully-Fisher relation was derived for this intermediate redshift sample, and it was found to have the same slope as the local T-F relation, but shifted 0.4 mag brighter. Thus, either the luminosities of the sample are higher or the masses of these galaxies lower than local disk galaxies.

The third DEEP galaxy sample consists of the U-band dropouts in the primary HDF that have confirmed redshifts $z > 2.2$, of which there are 12 galaxies (Lowenthal et al. 1997). The median

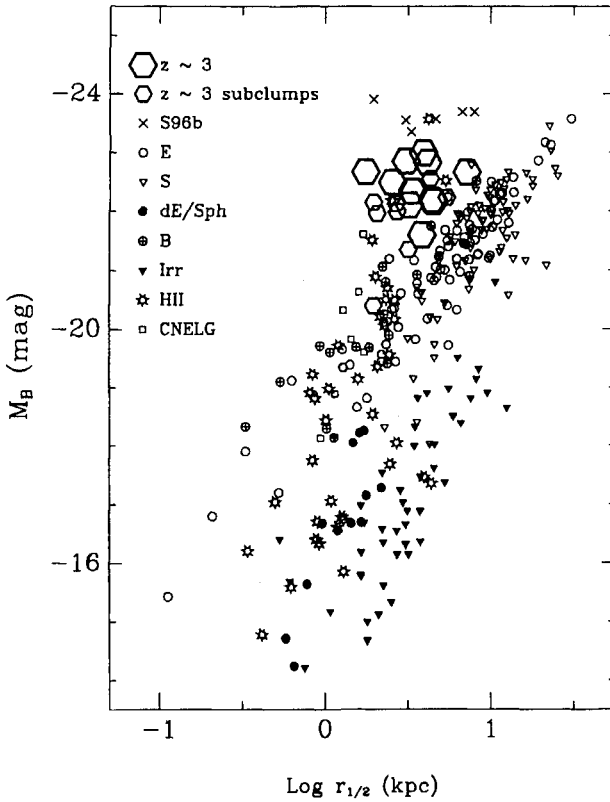


Figure 8. Half-light radii of the high-redshift sample of HDF galaxies (hexagons) vs. their blue luminosities, compared with various morphological types of galaxies at the present epoch. The high- z HDF objects have a mean radius of 3 kpc, and are more compact for their luminosities than any other types of galaxies (from Lowenthal et al. 1997).

optical luminosity of these galaxies is $2L_*$, thus they are not overly luminous, and their half-light radii are smaller than present epoch galaxies of their luminosity, as can be seen in Fig. 8. The median half-light radius of the sample is less than 4 kpc, so the luminous component of these galaxies is quite small and compact. The median redshift of the sample is $\langle z \rangle = 3.0$, and their averaged spectrum shows a blue continuum with characteristic ISM absorption lines, but quite weak $Ly-\alpha$ emission. The strengths of the UV absorption lines indicate low metallicity, and the combination of weak $Ly-\alpha$ with the very blue continuum suggests a moderate star formation rate coupled with dust.

What these U-band dropout systems are is difficult to say. They could be the early spheroids of present day massive elliptical galaxies, or they could represent the bulges of spirals. Perhaps they are sub-galactic clumps that will eventually merge to form the more massive systems of the present epoch. Whatever their evolutionary phase, they must be present today in some other form than we now observe them at high redshift because such compact systems of those luminosities are not observed at the present epoch.

8. Photometric Redshifts

The determination of the distances, i.e., redshifts, to the galaxies in the HDF is crucial to the interpretation of the data and to our understanding of the evolution of galaxies. The Keck 10m+LRIS is

capable of obtaining the spectra of galaxies down to about $R = 26^m$ with some effort, and therefore the faintest 3 magnitudes of galaxies in the HDF are beyond the limit at which we can reasonably expect to be able to measure redshifts spectroscopically in the coming decades. The possibility that approximate redshifts might be determined from broad-band photometry of the galaxies has therefore been explored by various groups, as has the identification of probable high-redshift galaxies based upon their broad-band colors.

The passage of the Lyman break through longer wavelength filter passbands for increasing redshifts produces a color signature in galaxies that is easy to identify. A sudden change in flux between two successive passbands is likely to be due to their placement on either side of the Lyman or Balmer discontinuities. Madau et al. (1996) have demonstrated that one can define regions in a 2-color diagram which are occupied by galaxies within a specific redshift range, and this procedure can be used to isolate galaxies within a redshift interval. Similarly, the Lyman break is redward of the U band for redshifts $z > 2.2$, and Steidel and colleagues (Steidel & Hamilton 1992; Steidel et al. 1996) have made use of this fact to define a sample of high redshift candidates which they have studied from the ground. This procedure has been used by various groups to define intermediate and high redshift samples of galaxies in the HDF.

One can carry this method further and use the observed fluxes of different types of galaxies, for which existing data are primarily confined to the present epoch, to determine what their broad band fluxes should be over a range of wavelengths and redshifts. A knowledge of the UV spectra of galaxies is necessary for this procedure since UV wavelengths are shifted into the optical at higher redshifts; therefore the observed IUE spectra of galaxies are essential data. Galaxy evolution models that predict how galaxy spectra evolve with time may be used to make corrections to local epoch spectra, and the effects of dust absorption may also be modeled and corrected for. With this information, templates of galaxy broad-band fluxes are constructed for different epochs, i.e., redshifts, and compared with the colors of individual galaxies measured from the HDF images in the four passbands. A redshift is assigned to each galaxy from the template that produces the smallest flux residuals, and a photometric redshift can be determined for any object having measurable broad-band fluxes.

A number of investigators have undertaken to refine the process of determining redshifts based upon broad-band colors or fluxes, and most of them utilize templates of galaxy spectra which they compare with the measured fluxes of the sample of galaxies (Gwyn & Hartwick 1996; Lanzetta et al. 1996; Mobasher et al. 1996; Sawicki, Lin, & Yee 1996). An alternative approach has been employed by Connolly et al. (1995), who fit polynomials to the observed spectra of galaxies of different redshift, using the measured spectra as a basis for the comparison with the sample of galaxies. An advantage of this method is that it does not depend on the assumption of template spectra for the basis set. A disadvantage is that it requires a calibrating set of galaxies with observed spectra, and very few exist in the regime $z > 0.5$.

A comparison of photometric redshifts determined for objects in the HDF with their spectroscopic redshifts is shown in Fig. 9 for two cases, viz., with and without an IR broad-band flux measurement. The inclusion of a flux point longward of 1μ is important to the accuracy of photometric redshifts because cool stars can mimic the spectral distribution of galaxies at moderate redshift if passbands in only the optical are used. The addition of one IR passband permits detection of the Balmer break at intermediate redshift, and resolves this degeneracy. One can see that the accuracy of photometric redshifts is greatly improved by the addition of an IR flux point. Hogg et al. (1998) conducted a blind test of predicted photometric redshifts vs. their Keck-measured spectroscopic redshifts for selected HDF galaxies, and their results are shown in Fig. 10. For redshifts in the range $z < 1$ the results are surprisingly good, and they demonstrate the validity of photometric redshifts to 10% accuracy.

9. Star Formation Rates

The use of photometric redshifts, which can be used to determine the approximate redshifts of even the faintest objects in the HDF, is central to the interpretation of the data and it opens up the HDF to important analysis of galaxy evolution. The luminosities of all objects imaged in the HDF are directly determinable for each of the passbands, as is the conversion of angular size to linear dimension. And, the variation with time, or epoch, of any quantity measurable from the

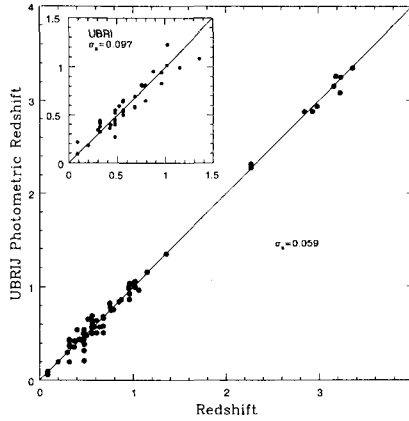


Figure 9. Keck-measured spectroscopic redshifts for galaxies in the HDF vs. photometric redshifts determined by Connolly et al. (1997).

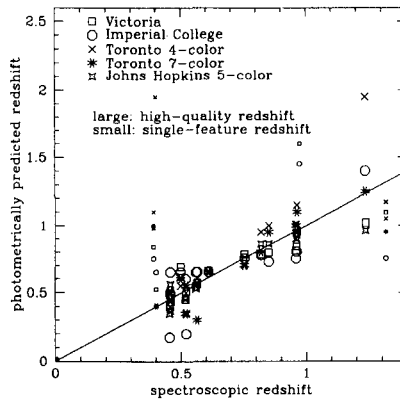


Figure 10. Blind test comparison of Keck 10m spectroscopic redshifts vs. photometric redshifts determined by different groups (from Hogg et al. 1998).

HDF can be determined, including the galaxy luminosity function, morphologies, space densities, interaction/merger rates, and star formation rates.

An example of fundamental information that can be obtained with photometric redshifts from the HDF is the derivation by Sawicki et al. (1996) of the galaxy luminosity function at different redshifts. By measuring the total brightness in the F450W filter of each galaxy they binned the data by redshift and derived the resulting luminosity function shown in Fig. 11. The bright end of the LF increases and the faint end steepens back to the epoch $z = 3$, after which the LF fades back to its low redshift value for $z = 4$.

Star formation rates (SFR) can also be determined as a function of redshift from the HDF, and this has produced one of the notable results from the Deep Field. Active star formation manifests itself by the presence of short-lived hot, luminous stars whose signatures are supernovae, H II regions, and a strong UV continuum. The rate of star formation is directly related via the initial mass function to the SNe rate, the $H\alpha$ and [O II] luminosities from H II regions, and the UV luminosity of the galaxy. All of these indicators have been calibrated for galaxies, and observation of any of them will yield a star formation rate. The HDF images in the various passbands provide

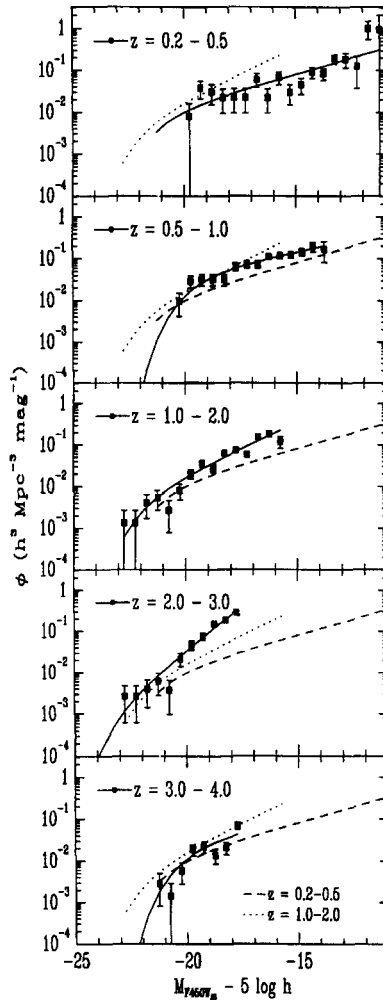


Figure 11. Evolution of the galaxy luminosity function with redshift for HDF objects, using photometric redshifts (from Sawicki, Lin, & Yee 1996).

the UV luminosities of galaxies for different redshifts, and these can be converted directly into the corresponding SFR at earlier epochs.

The local SFR at the present epoch has been determined from an $H\alpha$ objective prism survey of galaxies (Gallego et al. 1995), and an evaluation of star formation at intermediate redshifts has come from the ground-based Canada-France redshift survey (Lilly et al. 1996), whose magnitude-limited sample shows a steep rise in SFR with redshift out to $z = 1$. Madau et al. (1996) have used the HDF to probe the SFR for earlier epochs at $z > 1$ by using 2-color criteria to define U-, B-, and V-band dropouts, corresponding to galaxies with mean redshifts of 2.75, 4.0, and 5.5, respectively. They measured the mean UV luminosity of galaxies in each of these redshift intervals to derive the average SFR for that epoch. The results of all the above investigations enable the history of star formation to be pieced together, and is shown in Fig. 12.

A definite evolution of the SFR is apparent in which star formation begins modestly at high redshifts of $z > 4$, and increases to a maximum at epochs of $z \sim 1 - 2$. It then declines rapidly to

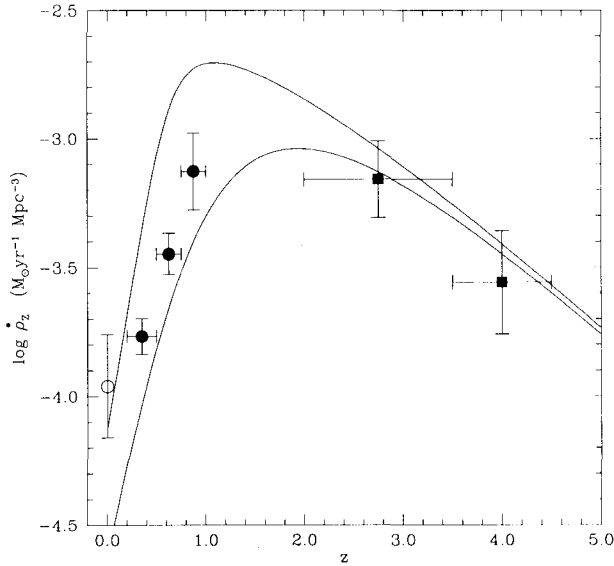


Figure 12. Global star formation rate (SFR) vs. redshift as determined from galaxy emission line strengths and UV continuum flux. The SFR's for $z < 1$ are derived from ground-based surveys, while $z > 1$ values are determined by Madau et al. (1996) from the HDF, and are uncertain because of the unknown effects of dust absorption. The solid curves are independent determinations from quasar absorption system abundances by Pei & Fall (1995).

the present time, such that the global SFR is now an order of magnitude lower than it was at its peak. This result is consistent with the Keck spectra of galaxies in the HDF, which show stronger [O II] and H I emission lines at intermediate redshifts of $z \sim 1$ than at higher or lower redshifts (cf. Guzman et al. 1997; Lowenthal et al. 1997). It should be noted that a separate determination of the SFR can be made from the IR fluxes of the HDF galaxies, caused by re-radiation of UV light by dust, and Rowan-Robinson has done this based on ISO data and concludes that the SFR for $z > 2$ may be substantially higher than that found by Madau et al.

It is significant that a totally independent determination of SFR history can be deduced from the abundances of the absorbing gas of damped $Ly-\alpha$ systems in quasars. Metal lines are detectable in the DLA systems and these should originate in the ISM of galaxies, so they track the SFR since heavy elements are created and injected into the ISM by the winds and explosions of massive stars. Heavy element abundances have been determined for the DLA's over a wide range in redshift, and the SFR is directly related to the change in abundance with redshift. Pei & Fall (1995) have analyzed the DLA abundances from models and have deduced the corresponding SFR with redshift. As their curves show in Fig. 12, their results are in quite good agreement with the SFR derived from the HDF. It thus appears that the HDF includes objects back at an epoch before most of the stars and galaxies now in existence had yet formed.

10. Summary

The Hubble Deep Field is a rich source of data encompassing both stellar and extragalactic astronomy. As further research on the HDF is performed using new techniques, new facts will emerge and some of the above results will need to be modified. The real significance of the HDF is its demonstration that by combining both space and ground-based telescopes we can now seriously study galaxies out to redshift $z > 3$ and down to 29th magnitude. After centuries of having to

confine study of the universe to local objects, it falls to us to live at a time when technology has developed the tools that enable us to address the most fundamental questions of our science: how the stars and galaxies now around us developed and evolved from the very first inhomogeneities that formed out of the early cosmic sea.

References

- Abraham, R.G. et al. 1996, *MNRAS*, **279**, L47
Cesarsky, C. et al. 1997, in preparation
Colley, W.N., Rhoads, J.E., Ostriker, J.P., & Spergel, D.N. 1996, *ApJ*, **473**, L63
Connolly, A.J. et al. 1995, *AJ*, **110**, 2655
Connolly, A.J., Szalay, A.S., Dickinson, M., Subbarso, M.U., & Brunner, R.J. 1997, *ApJ*, **486**, L11
Dickinson, M. 1995, in *Fresh Views of Elliptical Galaxies*, ed. A. Buzzoni, A. Renzini, A. Serrano, ASP Conf. Ser. No. 86, p. 283
Dressler, A., Oemler, A.J., Sparks, W.B., & Lucas, R.A. 1994, *ApJ*, **435**, 23
Elson, R.A.W., Santiago, B.X., & Gilmore, G.F. 1996, *New Astron*, **1**, 1
Ferguson, H.C. & Babul, A. 1997, *MNRAS*, in press
Fomalont, E.B., Kellermann, K.I., Richards, E.A., Windhorst, R.A., & Partridge, R.B. 1997, *ApJ*, **475**, L5
Fruchter, A.S., & Hook, R.N. 1997, in *Applications of Digital Image Processing*, ed. A. Tescher, Proc. SPIE, vol. 3164, in press
Gallego, J., Zamorano, J., Aragon-Salamanca, A., & Rego, M. 1995, *ApJ*, **455**, L1
Gould, A., Bahcall, J.N., & Flynn, C. 1997, *ApJ*, **482**, 913
Guzman, R. et al. 1997, *ApJ*, **489**, 559
Gwyn, S.D.J., & Hartwick, F.D.A. 1996, *ApJ*, **468**, L77
Hogg, D.W. et al. 1998, *AJ*, in press
Lanzetta, K.M., Yahil, A., & Fernandez-Soto, A. 1996, *Nature*, **381**, 759
Lilly, S.J., Le Fevre, O., Hammer, F., & Crampton, D. 1996, *ApJ*, **460**, L1
Lowenthal, J.D. et al. 1997, *ApJ*, **481**, 673
Madau, P. et al. 1996, *MNRAS*, **283**, 1388
Mendez, R.A., Minniti, D., De Marchi, G., Baker, A., & Couch, W.J. 1996, *MNRAS*, **283**, 666
Mobasher, B., Rowan-Robinson, M., Georgakakis, A., & Eaton, N. 1996, *MNRAS*, **282**, L7
Pei, Y.C. & Fall, S.M. 1995, *ApJ*, **454**, 69
Sawicki, M.M., Lin, H., & Yee, H.D.C. 1996, *AJ*, **113**, 1
Serjeant, S.B.G. et al. 1997, *MNRAS*, **289**, 457
Steidel, C.C. & Hamilton, D. 1992, *AJ*, **104**, 941
Steidel, C.C., Giavalisco, M., Dickinson, M., & Adelberger, K.L. 1996, *AJ*, **112**, 352
Vogt, N.P. et al. 1997, *ApJ*, **479**, L121
Williams, R.E. et al. 1996, *AJ*, **112**, 1335